Digest Journal of Nanomaterials and Biostructures Vol. 19, No. 4, October-December 2024, p. 1419-1433

Experimental and ab-initio analysis of structural, electronic and optical properties of ZMCO thin films elaborated by sol-gel method for optoelectronic application

R. Soudous*, A. Telia, A. Meziani, N. Nasri, L. Semra
Laboratory "Microsystems and Instrumentations (LMI)" of University of Constantine 1- Frères mentouri, Constantine 25000, Algeria

Thin $Zn_{0.9}Mg_{0.1-x}Cd_xO$ films have been deposited on a glass substrate by the sol gel dip coating method. The effects of cadmium and magnesium concentrations in the proportions of x= 0, 0.02, 0.04, 0.05, 0.06, 0.08, 0.1 on the structural and electronic properties of the elaborated layers have been studied. The micro structural, morphological, optical and electronic properties were analyzed experimentally by X-ray diffraction (XRD), Atomic Force Microscopy (AFM), ultraviolet-visible spectrophotometer (UV-vis) and current-voltage (I-V) measurements. Additionally, various parameters have been calculated by the density functional theory (DFT) using the Quantum Espresso code. The results show that all the deposited films develop a wurtzite crystal structure with grain size ranging from 12.3 nm to 18.9nm. The film transmittance was more than 80% in the visible range with band gap varying from 3.24eV to 3.45eV. The film surface was highly dense and homogenous without any cracks. With a ratio of about 1000, the photogenerated current is much higher in the presence of light than in the dark condition. The comparison between experimental and theoretical values showed the same parameters variations behaviors with a slight variation in the order of magnitude.

(Received August 6, 2024; Accepted October 4, 2024)

Keywords: ZnMgCdO, Thin films, Sol-gel, Quantum espresso, DFT, Optoelectronic properties

1. Introduction

The physical characteristics of the transparent conducting oxide (TCO) materials in the II-VI group have brought great interest in recent studies and research on semiconductors for the development of innovative devices. Among these materials, the zinc oxide (ZnO), which has an hexagonal wurtzite structure with high exciton binding energy of 60 meV, relatively wide direct band gap of 3.3eV at ambient temperature and high electron mobility [1, 2] allowing it to have a wide range of benefit, including their preparation, cost and safety. Zno has been already employed in ultraviolet optical devices such as: photoconductors [3], photodetectors [4, 5], solar cells [6] and light emitting diodes [7] as well as piezoelectric transducers [8] gaz and/or humidity sensors and biosensors [9-12]. The zinc oxide thin films can be elaborated by several deposition techniques, such as plasma enhanced chemical vapor deposition (PECVD) [13], atomic layer chemical vapor deposition (ALCVD) [14], physical vapor deposition (PVD) [15], spray pyrolysis technique [16] and sol-gel method [17].

The optical and electrical characteristics of undoped ZnO can be enhanced by introducing various elements such as Co [18], Cd [19], Al [20], Ga [21] and Mg [22]. The induced structural variations are beneficial to improve the ultra-violet emission performance and crystalline quality, transmittance in the visible range and smaller strains [23]. Among the ternary alloys of ZnO specifically $Zn_{1-x}Cd_xO$ has a narrow band gap (2.7eV), and $Zn_{1-x}Mg_xO$ has a larger band gap (>3.37) than of pure ZnO [24, 25]. This discrepancy is due to the differences in the ionic radius of Mg^{2+}(0.57Å), Cd^{2+}(0.97Å), and Zn^{2+}(0.60Å), it also makes the introduction of Mg atoms in the crystal structure easier than Cd atoms[26]. Incorporating Cd into the crystalline lattices can improve electrical conductivity by increasing the concentration of conduction electrons; however, the

* Corresponding author: redha.soudous@gmail.com
https://doi.org/10.15251/DJNB.2024.194.1419

integration of mg can improve optical transmittance due to defects reduction and crystallinity enhancement [27, 28].

In this work, the improvement of the electronic and optical properties of ZnO films by introducing Cd and Mg into the crystalline lattices has been investigated. Then, the effects of Cd and Mg concentrations on the ZnO optoelectronic properties have been analyzed. The importance of introducing both elements into the crystalline lattice of ZnO with a specific ratio that does not exceed 10% (to remain within the doping effect) is to obtain quaternary $Zn_{0.9}Mg_{0.1-x}Cd_xO$ (where x= 0, 0.02, 0.04, 0.05, 0.06, 0.08, 0.1). The sol-gel dip-coating technique has been used to elaborate thin films for several advantages such as: efficiency, flexibility, precise control over thickness, simplicity, low cost and low temperature processing and elaboration on various substrates. Structural characterization of the deposited layers has been carried out by X-ray diffraction (XRD) to determine the crystallographic structure, phase composition and other structural parameters. The ultraviolet-visible (UV-vis) transmittance has been used to measure the band gap (Eg) and light transmission in the ultraviolet and visible parts of the spectrum. The atomic force microscopy (AFM) has used to analyze the morphology of the surface layer and to measure various surface properties. The current-voltage (I-V) was measured to study the electrical properties of thin films in the ambient light and absolute darkness at room temperature. Additionally, the obtained experimental results have been compared to the calculated various parameters using the Density Functional Theory (DFT) method, adopting Quantum Espresso code. The DFT method is among the most commonly used approaches for "ab initio" electronic structure calculations.

2. Materials and methods

2.1. Experimental procedure

The quarter $Zn_{0.9}Mg_{0.1-x}Cd_xO$ ($0 \leq x \leq 0.1$) was synthesized, using the sol gel technique from zinc acetate dehydrate ($Zn(CH_3COO)_2.2H_2O$, ≥ 99%) as a precursor, 2-Methoxy ethanol ($C_3H_8O_2$, ≥ 99%) as a solvent and diethanolamine (DEA) ($C_4H_{11}NO_2$, ≥ 99%) as a stabilizer, magnesium chloride hexahydrate ($Cl_2Mg.6H_2O$, ≥ 98%) and cadmium acetate dehydrate ($Cd(CH_3COO)_2.2H_2O$, ≥ 99%) as the doping source. The solution was prepared by dissolving 0.5M concentration of zinc acetate dehydrate in a specified amount of solvent, then different amount of doping elements were added to the solution at several concentration of magnesium and cadmium which must be less than 10%. The chemical solution was mixed with a magnetic stirrer to obtain a white solution and to keep it more stable and transparent; the DEA was added subsequently with molar ratio of 1:1 to zinc acetate. After stirring ate 60°C for 2h on a hot plate, the solution was kept in a cold place for 24h. Before layers deposition, the glass substrates (CAT.NO.7105.1) were cleaned for 15min by acetone and ethanol in ultrasonic bath, then cleaned in distilled water and dried using optical paper. After each coating the moist thin films were preheated at 300°C for 10 min to evaporate the solvent (this procedure was repeated 10 times). Subsequently, the obtained samples were annealed in air for 2h at 500°C. The XRD analysis was carried out by using Burker D8 advance with copper X-ray tube (λ= 1.5406 Å) at 20 mA and 40kV to inspect the crystalline phase and orientation of Mg, Cd co-doped ZnO films. Optical transmittance measurements of the films were preformed using a dual-beam UV-vis spectrophotometer (UV-vis, 3 Shimadzu UV 336). Surface morphology of the thin films was analyzed by Atomic Force Microscope (AA2000 Atomic force Microscope, Angstrom Advanced Inc) and for current-voltage (I-V) measurements were studied using Keithley 487 Picommeter/voltage source.

2.2. Computational details

The first principle calculations of quaternary of $Zn_{0.9}Mg_{0.1-x}Cd_xO$ alloy in the wurtzite phase at different concentration (x= 0, 0.02, 0.04, 0.05, 0.06, 0.08, 0.1) were carried out by density functional theory (DFT) calculation using the Quantum Espresso code [29] for the structural and the electronic properties. The structural optimization was performed by using the generalized gradient approximation as proposed by Perdew-Burke-Ernzerhof [30] and the projected augmented wave (PAW) [31, 32] was employed to describe the interactions between the core and valence electrons of Zn, O, Mg and Cd atoms. The plane wave cut off energy set at 50 Ry and the electronic and ionic

energy convergence threshold at respectively 10^{-7} Ry and 10^{-4} Ry. The electronic properties of $Zn_{0.9}Mg_{0.1-x}Cd_xO$ were calculated using 2×2×2 gamma centered k-point grid for self-consistent calculation with a convergence energy threshold of 10^{-5} eV. To overcome the shortcoming of the GGA exchange-correlation functional in the gap energy calculation, the electronic properties were carried out with mBJLDA potential[33, 34]. This potential reproduces not only reasonably good energy gap values but at a lower time cost compared other time consuming functional. For the ternary $Zn_{0.9}Mg_{0.1}O$ and $Zn_{0.9}Cd_{0.1}O$, 20 atoms were used in the super cell structure, whereas 200 atoms were taken into account for the quaternary $Zn_{0.9}Mg_{0.1-x}Cd_xO$.

3. Results and discussion

3.1. Experimental results

3.1.1. XRD analysis

The XRD technique was used to examine the crystallinity, preferred orientation and in particular the impact of Mg and Cd doping on the crystal structure of the produced ZnO films. Diffraction peaks are described in figure 1 for different concentrations of Cd and mg. Comparing the XRD peaks with JCPDS data sheet (card file no: 36-1451, Zincite phase) [35], three main distinct peaks corresponding to planes (100), (002) and (101) at approximate 2θ values of 31.9, 34.5 and 36.4 degrees, respectively have been observed for each sample, where the highest one is (101) plane. This observation suggests that the films exhibit a hexagonal wurtzite structure with a preferred orientation along the (101) plane and it can also be noticed that the intensity of the diffracted peaks has changed with the change of Mg and Cd concentrations [26].

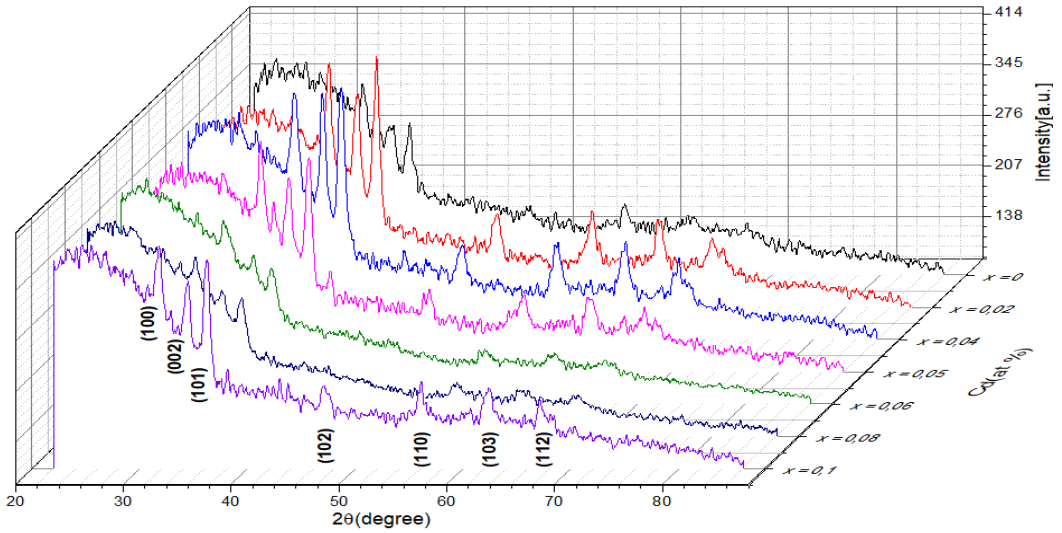

Fig. 1. XRD patterns of $Zn_{0.9}Mg_{0.1-x}Cd_xO$ thin films for ($0 \leq x \leq 10\%$).

The average grain size (D) of $Zn_{0.9}Mg_{0.1-x}Cd_xO$ thin films was calculated using the Debye-Scherrer equation [36]:

$$D = (0.94 \times \lambda)/(\beta \cos\theta) \quad (1)$$

where λ represents the wavelength of the X-ray (λ=0.15406nm), β denotes the Full Width at Half Maximum (FWHM) in radians and θ is the angle of diffraction according to Bragg's law. Additionally, the lattice constants (A, c) were determined using the following formula [37, 38]:

$$1/(d_{hkl})^2 = (4/3)\left((h^2 + hk + k^2)/a^2\right) + l^2/c^2 \quad (2)$$

$$a = \lambda/(\sqrt{3}\ sin\theta\ ) \quad (3)$$

$$c = \lambda/(sin\ \theta) \quad (4)$$

where d represents the inter-planar distance h, k, l are the Miller indices. The position parameter (u) was determined using the specified equation [38]:

$$u = a^2/3c^2 + 0.25 \quad (5)$$

The average crystallite size (D), the lattice constants (a, c), the ratio c/a and the position parameter (u) were calculated from the formulas mentioned above. The results obtained were summarized in Table 1. It is noted that if the cadmium content increases the concentration of magnesium decreases because the sum of the co-dopant contents is 10%. It can be explained by the difference in the chemical binding properties of MgO and CdO compared to that of ZnO. The results indicated as well that with the increase of Cd concentration, the lattice parameters (a, c) incrase from 3.2Å to 3.25Å and from 5.14Å to 5.2Å respectively. These results are comparable to those obtained by J Jassi *et al* [10] on $Zn_{0.9}Cd_{0.1}O$, Yongli Li *et al* [26] on $Zn_{0.9}Mg_{0.1}O$ and Onyekachi Kalu *et al* [39, 40] on CZMO thin films grown at Rf power on silicon (100) substrates at room temperature. Concerning the grain size (D), their values decrease from 18.9 nm to 12.3 nm when Cd contents increase. These grain size values have the same order of magnitude with those obtained on CdMgZnO nanoparticles synthesized by sol-gel method [41]. The values of the position parameter (u) and the ratio c/a are identical to the theoretical ZnO values in the ideal hexagonal wurtzite phase (0.375) and (1.63) [42].

Table 1. The lattice parameters of $Zn_{0.9}Mg_{0.1-x}Cd_xO$ ($0 \leq x \leq 10\%$) thin films determined from (002).

Cd content (x)	**2θ(°)value (002)**	**FWHM β(°)**	**D (nm)**	**Lattice parameters**				**c/a ratio**	**u**
				a(Å)	**c(Å)**	**a(Å) other works**	**c(Å) other works**		
0.00	34.9140	0.4609	18.872	3.2023	5.1355	3.244 [26]	5.217 [26]	1.6037	0.3796
0.02	34.6199	0.5447	15.956	3.2249	5.1778	/	/	1.6056	0.3793
0.04	34.5176	0.6030	14.409	3.2335	5.1926	/	/	1.6059	0.3793
0.05	34.5077	0.6345	13.693	3.2361	5.1941	/	/	1.6051	0.3794
0.06	34.5006	0.6392	13.592	3.2386	5.1951	/	/	1.6041	0.3795
0.08	34.4819	0.6986	12.436	3.2436	5.1979	/	/	1.6025	0.3798
0.10	34.4674	0.7060	12.305	3.2470	5.1999	3.23 [10]	5.18 [10]	1.6014	0.3799

The atomic packing fraction (APF), cell volume (V), bond length (L) and degree of distortion (R) were also evaluated using the following equations [41]:

$$APF = 2\pi a/\left(3\sqrt{3}c\right) \quad (6)$$

$$V = \left(\sqrt{3}/2\right)a^2\ c \quad (7)$$

$$L = \sqrt{((a^2\ /\ 3) + (1\ /\ 2 - u)^2\ c^2\ )} \quad (8)$$

$$R = \left(2a\sqrt{2/3}\right)/c \quad (9)$$

The film stress was evaluated using the following equation:

$$\sigma = \left(\left(2(C_{13})^2 - C_{33}(C_{11} + C_{12})\right)/2C_{13}\right) \times \left(\left(C_{film} - C_0\right)/C_0\right) \quad (10)$$

where the elastic constants C_{ij} for single crystal ZnO are typically represented by set of numerical values: C_{33}=213.8GPa, C_{13}=104.2GPa, C_{12}=119.7GPa and C_{11}=208.8GPa. Whereas C_{film} represents the lattice constant of the c-axis for the quaternary $Zn_{0.9}Mg_{0.1-x}Cd_xO$ ($0 < x \leq 10\%$) thin film, where C_0=0.51978nm denotes the unstrained lattice parameter of ternary $Zn_{0.9}Mg_{0.1}O$ i.e. (x=0) [39, 43].

Table 2 summarizes the atomic packing fraction, the cell volume, the bond length, the degree of distortion and the stress for cadmium contents, calculated from equations (6), (7), (8), (9) and (10), respectively. It can be noticed that the cell volume exhibits a modest expansion from 45.61 Å^3 to 47.48 Å^3, while the degree of distortion shows minimal variation (R≈1.02) despite the increased (x) content. Furthermore, the atomic packing fraction shown a slight increase from 75.36 to 75.47 and the bond length extends from 1.95 Å to 1.98 Å. The values determined exhibit a similar magnitude compared to those reported by Onyekachi kalu *et al* [41] in their study on CdMgZnO nanoparticles. Also, the stress appears to decrease from -1.92 GPa to -2.92 GPa (become more negative) as the cadmium content increases. A negative stress value often indicates a state of compression, with values similar to those described in the reference [39]. Although the values of all parameters are close when cadmium and magnesium are added to ZnO cell elements, a slight change can be noticed in the characteristics of the structure, which further improves its crystallinity. The values of all parameters deduced for quaternary $Zn_{0.9}Mg_{0.1-x}Cd_xO$ are between those of ZnMgO (x=0) and ZnCdO (x=0.1).

Table 2. Cell volume (V), degree of distortion (R), atomic packing fraction (APF), bond length (L) and stress (σ) for $Zn_{0.9}Mg_{0.1-x}Cd_xO$ ($0 \leq x \leq 10\%$) thin films.

Cd content (x)	V (Å^3)	R	APF	L (Å)	Stress(σ) (GPa)
0.00	45.6067	1.0183	75.3633	1.9495	0
0.02	46.6335	1.0171	75.2756	1.9640	-1.9165
0.04	47.0179	1.0169	75.2606	1.9694	-2.5909
0.05	47.1045	1.0174	75.2983	1.9706	-2.6566
0.06	47.1887	1.0180	75.3432	1.9718	-2.7032
0.08	47.3573	1.0190	75.4182	1.9741	-2.8270
0.10	47.4789	1.0197	75.4687	1.9759	-2.9233

Figure 2(a) shows the evolution of the lattice parameters (a, c) as a function of the cadmium content. It has been observed that their values increase rapidly in the range of $0 \leq x \leq 0.04$ and increase slowly beyond $x \geq 0.05$. this variation is probably due to the substitution of Mg^{2+} ions by Cd^{2+} ions in the lattice sites, knowing that the ionic radii of Cd^{2+} is relatively large (0.97Å) than the ionic radii of Mg^{2+}(0.57Å) and Zn^{2+}(0.60Å). The increase of the lattice parameters (a, c) by increasing Cd concentration has been also observed by Onyekachi Kalu *et al* [39] in CdMgZnO films obtained by RF sputtering with different Cd concentrations. The cell volume and grain size represented in Figure 2(b) indicate an increase in the volume size and a decrease in the grain size with increasing the Cd content due to the increase of the lattice parameters (a, c). This behavior has been also observed by Aouacheria *et al* [22] in the ternary $Zn_{1-x}Mg_xO$ when increasing the Mg concentration. The variation of the positional parameter (u) and the ratio c/a are shown in Figure 2(c). It can be noted that at x=0.04 an inflection point is considered. It is observed that the position parameter (u) decreases with increasing the cadmium concentration until x=0.04, then it continues to increase by increasing the concentration x to 0.1. However, for the ratio c/a, the opposite evolution has been observed. Figure 2(d) shows the variation of the atomic packing fraction and the degree of distortion, where their variations are identical to that observed for the position parameter (u). The degree of distortion can be influenced by several factors, such as atomic interactions and the presence of defects or dislocations. The observed variation could reflect localized changes in

atomic arrangements or internal deformations [44]. For the atomic packing fraction, the cause of this variation is the addition of new atoms or groups, which can disrupt the effective packing, reduce the APF, but as the structure adjusts, it can regain or even improve its packing [38]. The bond length and the stress are shown in Figure 2(e), it can be seen that the bond length increases with the increase in cadmium content (x). on the other hand, the stress (becomes more negative) could be due to the introduction of Cd and Mg atoms with different sizes or electro negativities, which modifies the equilibrium distances between the atoms and it results in a more compressive stress in the lattice [41].

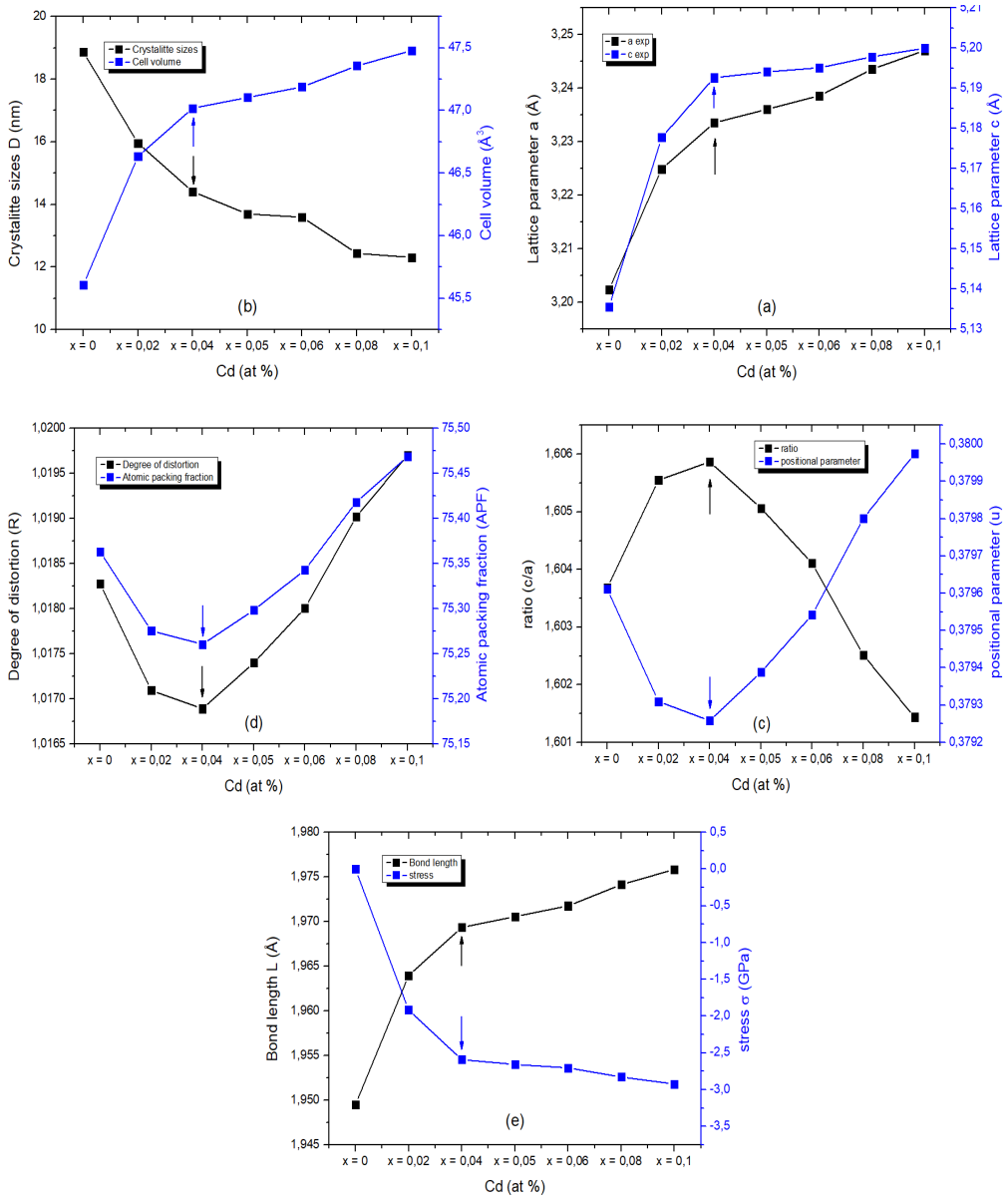

Fig. 2. (a) Lattice constant (a, c) variation with x content, (b) variation in cell volume and crystallite size of $Zn_{0.9}Mg_{0.1-x}Cd_xO$ for ($0 \leq x \leq 10\%$), (c) variation of the position parameter (u) and c/a ratio with the increase in x content, (d) correlation between atomic packing fraction (APF) and degree of distortion (R) for $Zn_{0.9}Mg_{0.1-x}Cd_xO$ ($0 \leq x \leq 10\%$) and (e) bond length (L), stress (σ) as a function of x content.

3.1.2. Surface morphology

The 2D and 3D surface morphology of 3000 nm × 3000 nm scanning region of $Zn_{0.9}Mg_{0.1-x}Cd_xO$ thin films are shown in Figure 3. On close inspection of the AFM image, it was noticed that with the increase of Cd concentration, the grain size became smaller and the surface were highly dense and homogeneous without any cracks. This observation could be due to the presence of Cd^{2+} ions that will occupy the vacant pores and accumulate on the surface that reduces the dispersion of light on the surface [45, 46]. Through AFM analysis, the root mean square (Rms) and average roughness (Ra) were calculated and summarized in Table 3. It can be observed that when the cadmium content increases, the Ra and Rms decrease from 4.5 nm to 2.22 nm and from 5.46 nm to 2.78 nm respectively.

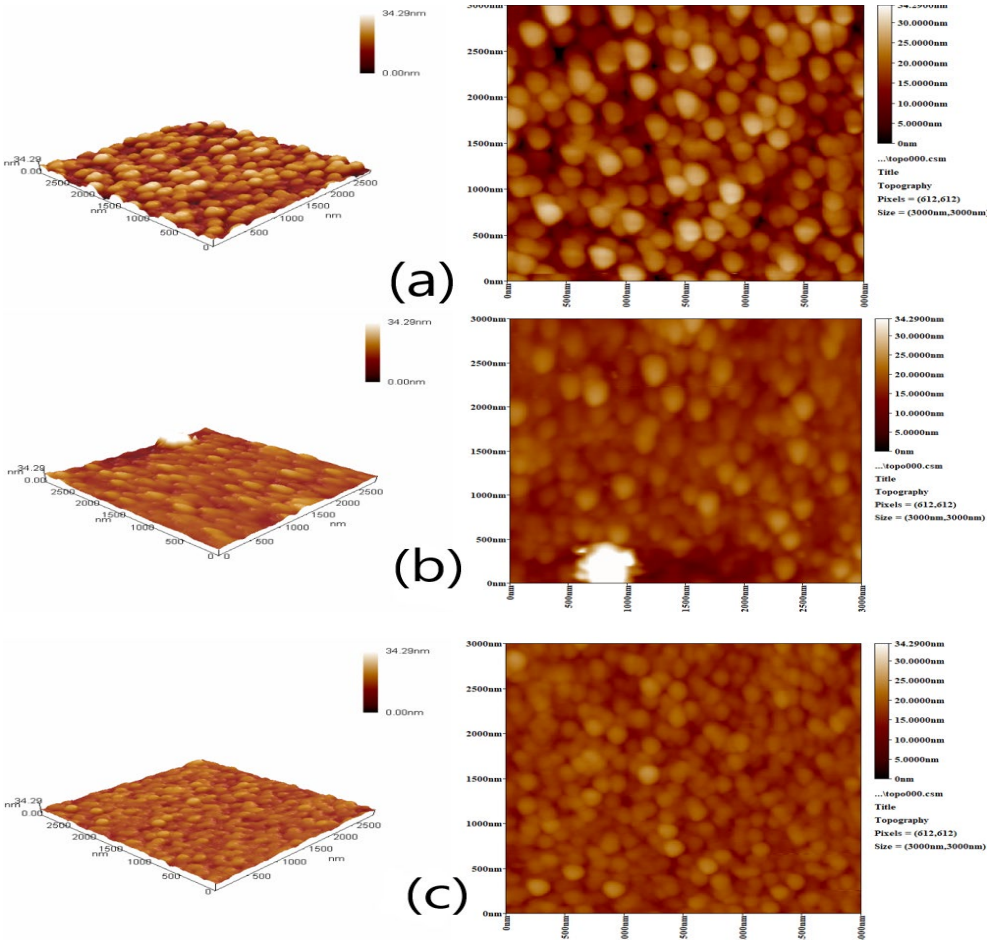

Fig. 3. 2D and 3D AFM images of $Zn_{0.9}Mg_{0.1-x}Cd_xO$ ($0 \leq x \leq 10\%$) thin films (a) x=0%, (b) x=5%, (c) x=10%.

Table 3. The root mean square (Rms) and the average roughness (Ra) of $Zn_{0.9}Mg_{0.1-x}cd_xO$ ($0 \leq x \leq 10\%$) thin films.

Cd content (x)	Rms (nm)	Ra (nm)
0.00	5.46	4.5
0.05	3.23	2.71
0.10	2.78	2.22

3.1.3. UV-vis spectroscopy

Figure 4 shows the transmittance spectra of co-doped ZnO films measured in the wavelength range of 300-850nm. In general, $Zn_{0.9}Mg_{0.1-x}Cd_xO$ films have a transmittance more than 80% in the visible rang, signifying its transparency within this range. With the presence of sharp cut-off at ultraviolet (UV) in wavelength region between 340nm and 375nm demonstrating high UV light absorption [35].

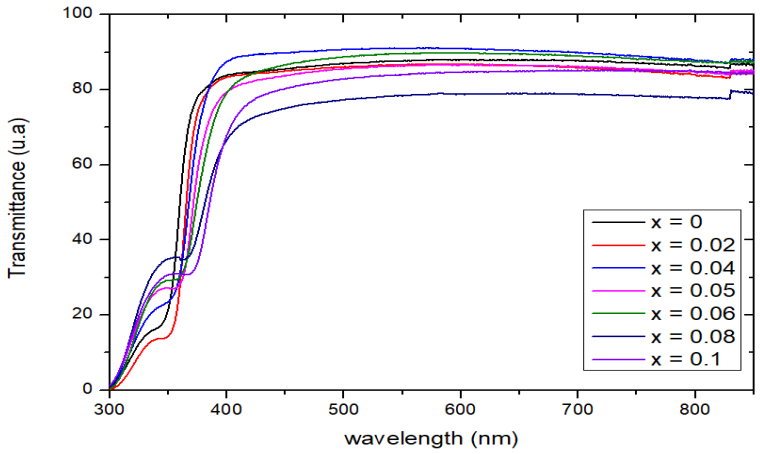

Fig. 4. Optical transmittance of $Zn_{0.9}Mg_{0.1-x}Cd_xO$ ($0 \leq x \leq 10\%$) thin films.

There are different proven methods for measuring approximately the optical band gap. In this work, we have used the method described in the reference [47]. Figure 5 shows the derivative of the transmittance of $Zn_{0.9}Mg_{0.1-x}Cd_xO$ versus energy at different Cd concentration. The spectra show that when the cadmium content decreases, the shape of the peak becomes narrower and deeper.

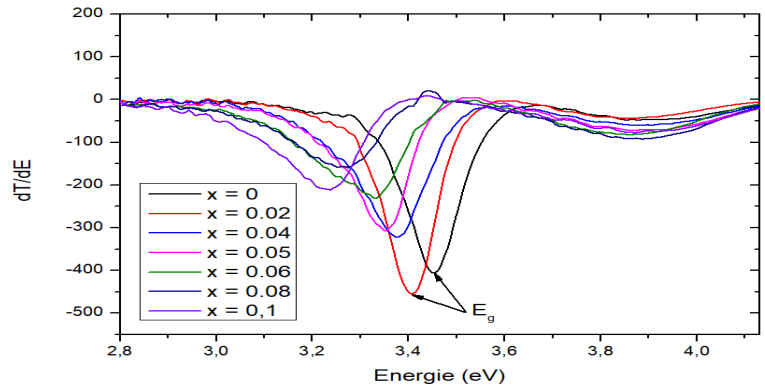

Fig. 5. Transmittance derivative spectra of $Zn_{0.9}Mg_{0.1-x}Cd_xO$ ($0 \leq x \leq 10\%$) thin films

The optical band gap was determined from the minimum in the first order derivative of transmittance spectra. The obtained results are summarized in Table 4. It can be observed that the band gap energy decreases when the Cd concentration increases, due to the integration of Cd atoms in the structure, which can introduce new energy levels within the band gap or alter the band edges, leading to a narrower gap between the valence and conduction bands [48]. These results can be compared to those reported by J Jassi *et al* [10] on $Zn_{0.9}Cd_{0.1}O$ and Yongli Li *et al* [26] on $Zn_{0.9}Mg_{0.1}O$.

Table 4. Band gap energy of $Zn_{0.9}Mg_{0.1-x}Cd_xO$ ($0 \leq x \leq 10\%$) thin films.

Cd content (x)	Band gap energy E_g (eV)	
		other works
0.00	3.4536	3.35 [23]
0.02	3.4061	/
0.04	3.3783	/
0.05	3.3513	/
0.06	3.3291	/
0.08	3.2754	/
0.10	3.2361	3.14[9]

3.2.4. Current-voltage measurements (I-V)

The current-voltage (I-V) characteristics obtained at room temperature under light and dark conditions for $Zn_{0.9}Mg_{0.1-x}Cd_xO$ thin films in metal-semiconductor-metal (MSM) configuration are presented in Figure 6. The silver [7] is the metal electrode and $Zn_{0.9}Mg_{0.1-x}Cd_xO$ is the semiconductor. The current-voltage measurements were recorded in the range of $-5V \leq V \leq +5V$ for thin films elaborated with various Cd concentrations ($0 \leq x \leq 10\%$). Figure 6(a) shows the current-voltage (I-V) obtained under illumination where a linear evolution was observed.

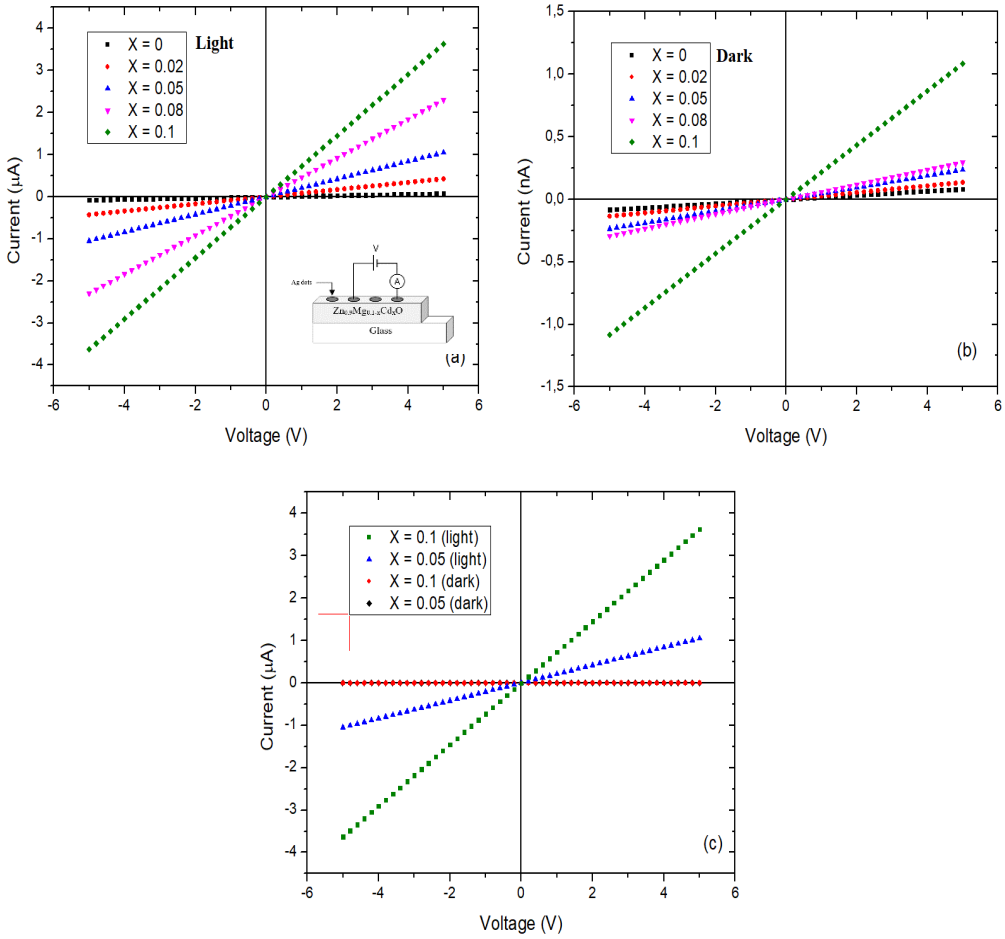

Fig. 6. Current-voltage characteristics obtained for $Zn_{0.9}Mg_{0.1-x}Cd_xO$ ($0 \leq x \leq 10\%$) thin films. (a) under light condition with the schematic set-up of I-V measurements, (b) in dark condition, (c) comparison between light and dark condition.

This good linearity suggests that ohmic contacts are formed at the metal-semiconductor interfaces. This behavior was observed by S.Sharma *et al* [4] on Al/CZO/Al and P.S.Shewale *et al* [49] on Al/MZO/Al device. This result indicates that the introduction of Cd elements in the ZnMgO structure improves the photogenerated current while preserving the nature of the contact under illumination. Figure 6(b) displays the variation of the current in dark conditions. A low generate current of the order of (nA) for all Cd concentrations has been measured. However, the increase in Cd content does not significantly affect the dark current, indicating that the intrinsic conductivity of ZnMgO does not change much further. The (I-V) curves for x=0.05 and x=0.1 under light and dark conditions are presented in Figure 6(c).

A significant difference in current values with a higher ratio in the order of 1000 was observed between currents under illumination and dark conditions. This is likely due to Cd acting as a dopant, which creates additional energy states within the band gap, facilitating the generation of electron-hole pairs when exposed to light. From these observations, we may conclude that the introduction Cd atoms in the ZnMgO structure, enhances the sensitivity to light.

3.3. Computational results

3.3.1. Structural properties

Table 5 summarizes the results obtained with Quantum Espresso code of the structural parameters (a, c) calculation in the wurtzite phase of quaternary compounds $Zn_{0.9}Mg_{0.1-x}Cd_xO$ under various Cd contents. The other parameters were deduced from the formulas mentioned above. The calculated values from the position parameter (u) and the ratio c/a are approximately equal to the ZnO theoretical values in the ideal hexagonal wurtzite phase, which are in the order of 0.375 and 1.63, respectively [42].

Table 5. Optimized crystallographic parameter of quaternary $Zn_{0.9}Mg_{0.1-x}Cd_xO$ ($0 \leq x \leq 10\%$) in wurtzite structure.

Cd content (x)	Lattice parameters a (Å)	c(Å)	Ratio c/a	V (Å^3)	R	APF	L	u	Stress(σ) (GPa)
0.00	3.2773	5.2693	1.6078	49.0121	1.0157	75.1694	1.9968	0.3789	0
0.02	3.2837	5.2823	1.6086	49.3251	1.0151	75.1308	2.0010	0.3788	-0.5744
0.04	3.2900	5.2982	1.6104	49.6636	1.0140	75.0491	2.0055	0.3785	-1.2769
0.05	3.2941	5.3017	1.6095	49.8203	1.0146	75.0930	2.0077	0.3787	-1.4315
0.06	3.2959	5.3090	1.6108	49.9435	1.0138	75.0307	2.0093	0.3785	-1.7541
0.08	3.2993	5.3204	1.6126	50.1540	1.0127	74.9472	2.0121	0.3782	-2.2577
0.10	3.3007	5.3306	1.6150	50.2928	1.0111	74.8355	2.0139	0.3778	-2.7084

The lattice parameters (a, c), the cell volume and bond length calculated are plotted in the Figures 7(a) and 7(b), respectively as a function of Cd content. The calculated values of (a, c), cell volume and bond length present nearly the same variations behavior and the same order of magnitude with those deduced experimentally. The Figure 7(c) illustrates the fluctuation of the ratio c/a and the position parameter (u). The atomic packing fraction (APF) and degree of distortion (R) are shown in figure 7(d).

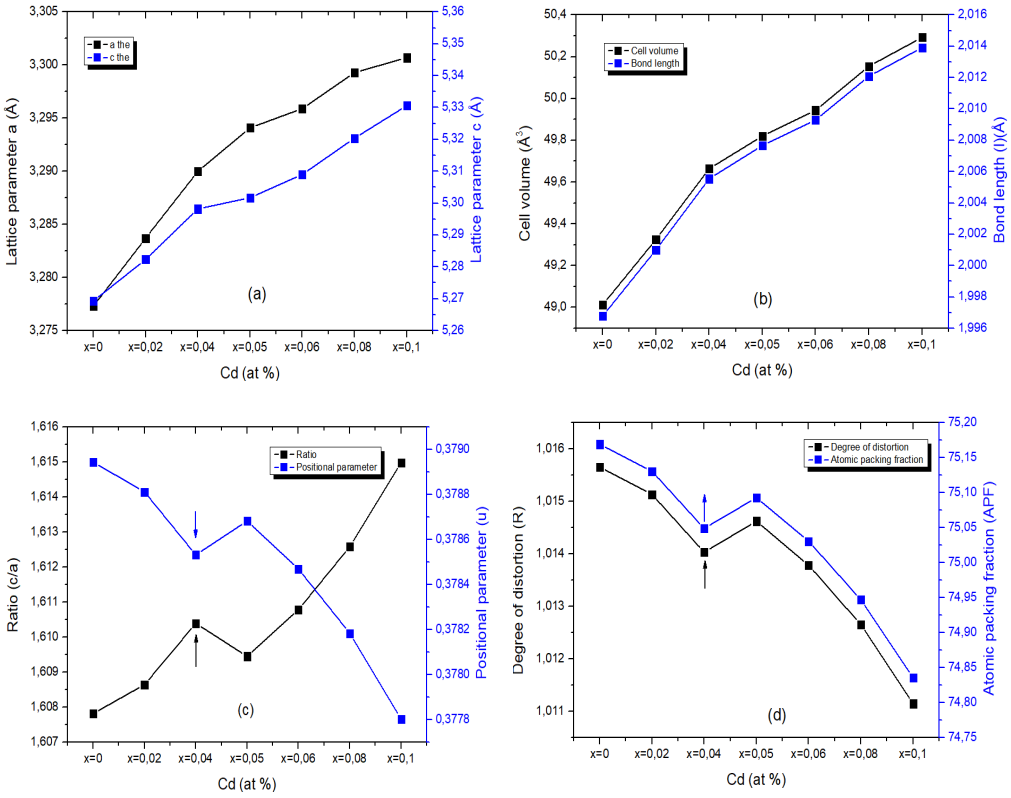

Fig. 7. (a) Lattice constant (a, c) variation with x content in wurtzite structure, (b) variation of cell volume (V) and bond length (L) of $Zn_{0.9}Mg_{0.1-x}Cd_xO$ ($0 \leq x \leq 10\%$) in wurtzite phase, (c) variation in position parameter (u) and c/a ratio of $Zn_{0.9}Mg_{0.1-x}Cd_xO$ ($0 \leq x \leq 10\%$) in wurtzite composition, (d) correlation between atomic packing fraction (APF) and degree of distortion (R) with increase in x content in wurtzite phase.

3.3.2. Electronics properties

Table 6 summarizes the $Zn_{0.9}Mg_{0.1-x}Cd_xO$ band gap DFT calculation for different contents in the wurtzite phase. It can be seen that the band gap obtained decreases when the Cd concentration increases the band gap [10] values varied between 2.92eV and 2.23eV, which correlates well with the band gap behavior observed experimentally.

Table 6. Band gap energy of $Zn_{0.9}Mg_{0.1-x}Cd_xO$ ($0 \leq x \leq 10\%$) in wurtzite structure.

Cd content (x)	**Band gap energy E_g (eV)**
0.00	2.9212
0.02	2.7202
0.04	2.5259
0.05	2.4680
0.06	2.4413
0.08	2.4058
0.10	2.2280

3.4. Comparative results

The lattice parameters (a, c) derived from experimental measurements compared to those calculated using Quantum Espresso were presented in Figure 8(a). The computed and the experimental values of the lattice constants (a, c) are very close and increase with increasing Cd contents. Figure 8(b) shows the comparison between the calculated and experimental values of the c/a ratio and the position parameter (u), which shows very close values and small variation. Figures 8(c) and 8(d) show a comparative analysis between experimental and theoretical values of the cell volume, the atomic packing fraction, the degree of distortion and the bond length. A slight difference of about 5 $Å^3$ has been observed for the cell volume, whereas the experimental and theoretical results are very close for the atomic packing fraction, the degree of distortion and the bond length. Figure 8(e) displays the comparison concerning stress levels (σ) which shows a similarity the order of magnitude.

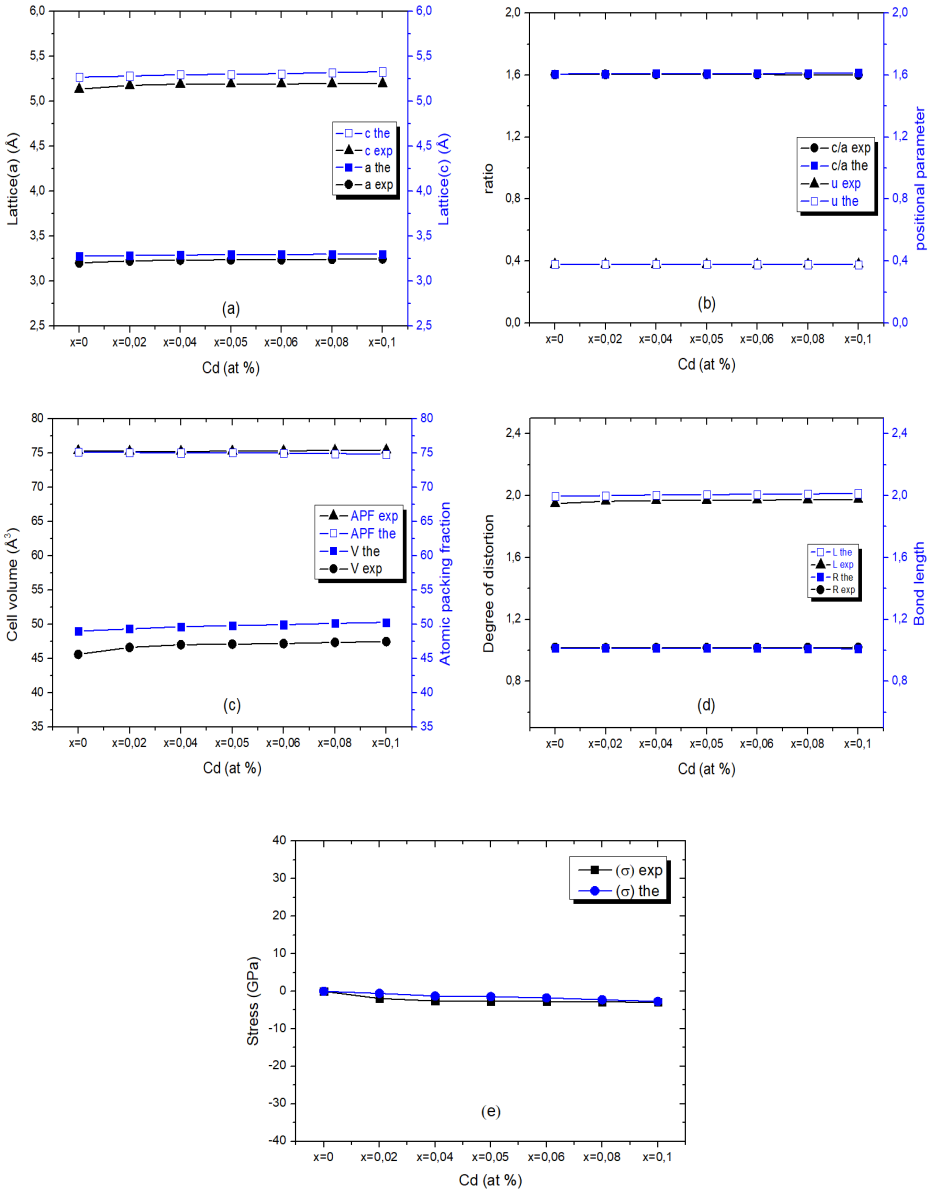

Fig. 8. The experimental and theoretical crystallographic parameter of $Zn_{0.9}Mg_{0.1-x}Cd_xO$ ($0 \leq x \leq 10\%$) (a) Lattice constant (a, c), (b) Position parameter (u) and ratio c/a, (c) Cell volume (V) and atomic packing fraction (APF), (d) Degree of distortion (R) and bond length (L), (e) stress (σ).

Figure 9 shows the results of the band gap energy [10] deduced by the theoretical DFT methods and obtained experimentally, where only slight deviation is observed.

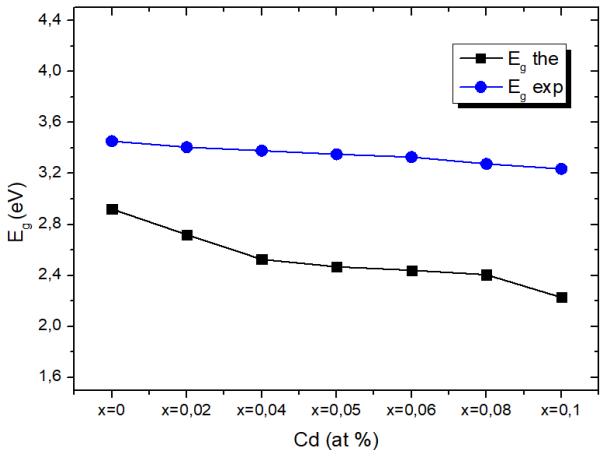

Fig. 9. The experimental and theoretical band gap energy of $Zn_{0.9}Mg_{0.1-x}Cd_xO$ ($0 \leq x \leq 10\%$).

4. Conclusion

In this study, $Zn_{0.9}Mg_{0.1-x}Cd_xO$ thin films with different concentrations of cadmium and magnesium have been synthesized using the sol-gel dip-coating technique. The structural, morphological, optical and electronic properties have been analyzed by XRD, AFM, UV-visible and current-voltage (I-V) characterizations technique, respectively. To corroborate the obtained results, the various parameters have been computed using the DFT method, adopting Quantum Espresso code. Compared to experimental results, the theoretical results show a slight change in the values of the different parameters, with the same variation behavior. XRD analysis revealed a wurtzite crystal structure with more surface cohesion and no defects or cracks, due to Mg and Cd atoms replacing Zn atoms, permitting less light dispersion. A higher transmission of visible light ($T \geq 75\%$) and more absorption of ultraviolet rays ($T \geq 40\%$) were observed with an energy gap confined between $3.33 \leq E_g \leq 3.45$.

The photogenerated current in the presence of light is significantly increased by a ratio of about 1000. From the results analysis, we may conclude that the lattice constants (a, c) of ZnMgO are smaller than those of ZnCdO, resulting in a smaller size and greater volume cell, which improves optical properties. Concerning electronic properties, ZnCdO has a lower energy gap due to a closer valence and conduction level. Analysis of $Zn_{0.9}Mg_{0.1-x}Cd_xO$ thin films (I-V) characteristics in MSM configuration shows that the increase in Cd content improves the photogenerated current under light conditions while maintaining low currents in the dark. This observation makes $Zn_{0.9}Mg_{0.1-x}Cd_xO$ thin films promising candidates for optoelectronic application where high sensitivity to light with low dark current is essential. ZnMgCdO possesses the properties of the both ZnMgO and ZnCdO depending on the proportion of Mg and Cd added to the ZnO mixture.

Acknowledgments

This research was funded by the DGRSDT and the Laboratory "Microsystémes et Instrumentation (LMI)" of the university Constantine 1- Fréres Mentouri, Algeria.

References

[1] M. Rouchdi, E. Salmani, B. Fares, et al., Results in Physics. vol.7, p.620-627 (2017); http://doi.org/10.1016/j.rinp.2017.01.023
[2] G. Gupta, S. Rath, Materials Today: Proceedings. vol.67, p.263-266 (2022); https://doi.org/10.1016/j.matpr.2022.07.274
[3] M. Kumar, V. Bhatt, A. C. Abhyankar, et al., Sensors and Actuators A: Physical. vol.270, p.118-126 (2018); https://doi.org/10.1016/j.sna.2017.12.045
[4] S. Sharma, M. Tomar, V. Gupta, et al., Superlattices and Microstructures. vol.151, p.106812 (2021); https://doi.org/10.1016/j.spmi.2021.106812
[5] M. Jabeena, M. Asharaf, S. Tayyabad, et al., Dig. J. Nanomater. Biostruct. vol.16, p.1253-1261 (2021).
[6] J. Cortazar, A. L. Matus, L. R. Blanco, et al., Digest Journal of Nanomaterials & Biostructures (DJNB). vol.19, p.493-502 (2024); https://doi.org/10.15251/DJNB.2024.192.493
[7] N. N. Mude, H. I. Yang, T. T. Thuy, et al., Organic Electronics. vol.112, p.106696 (2023); https://doi.org/10.1016/j.orgel.2022.106696
[8] X. Zhang, H. Wu, Y. Zhang, et al., Journal of Materiomics, (2024); https://doi.org/10.1016/j.jmat.2024.02.009
[9] S. Ghanem, A. Telia, C. Boukaous, et al., International Journal of Nanotechnology. vol.12, p.697-707 (2015); https://doi.org/10.1504/IJNT.2015.068890
[10] J. Jassi, M. Sara Roy, M. Sreelakshmi, Materials Today: Proceedings (2023); https://doi.org/10.1016/j.matpr.2023.11.070
[11] H. A. Wahab, A. A. Salama, A. A. El-Saeid, et al., Results in Physics. vol.3, p.46-51 (2013); https://doi.org/10.1016/j.rinp.2013.01.005
[12] S. Jubear, O. Abdulmunem and E. Hassan, Digest Journal of Nanomaterials & Biostructures (DJNB). vol.19, p.97-106 (2024); https://doi.org/10.15251/DJNB.2024.191.97
[13] P. Hu, N. Han, D. Zhang, et al., Sensors and Actuators B: Chemical. vol.169, p.74-80 (2012); https://doi.org/10.1016/j.snb.2012.03.035
[14] Z.-H. Li, E.-S. Cho and S. J. Kwon, Applied Surface Science. vol.314, p.97-103 (2014); https://doi.org/10.1016/j.apsusc.2014.06.136
[15] L. Wang, X. Zhang, S. Zhao, et al., Applied Physics Letters. vol.86, (2005); http://dx.doi.org/10.1063/1.1851607
[16] A. Alasmari, A. A. Awad, A. A. Aboud, Optical Materials. vol.148, p.114899 (2024); https://doi.org/10.1016/j.optmat.2024.114899
[17] S. Anandhi, A. Sagaya Amala Immanuel, V. Ramkumar, et al., Materials Today: Proceedings (2023); https://doi.org/10.1016/j.matpr.2023.06.232
[18] J. M. Ashfaq, B. C. Hu, N. Zhou, et al., Journal of Luminescence. vol.158, p.211-214 (2015); https://doi.org/10.1016/j.jlumin.2014.09.048
[19] S. Wu, X. Cheng, X. Rong, et al., Journal of Luminescence. vol.248, p.118945 (2022); https://doi.org/10.1016/j.jlumin.2022.118945
[20] S. M. Al-Sofiany, H. E. Hassan, A. H. Ashour, et al., International Journal of Electrochemical Science. vol.9, p.3209-3221 (2014); https://doi.org/10.1016/S1452-3981(23)08004-5
[21] H. B. Cuong, C.-S. Lee, S.-H. Jeong, et al., Acta Materialia. vol.130, p.47-55 (2017); https://doi.org/10.1016/j.actamat.2017.03.033
[22] F. Z. Aouacheria, A. Telia, R. Soudous, et al., Micro and Nanostructures. vol.164, p.107155 (2022); https://doi.org/10.1016/j.spmi.2022.107155
[23] L. Xu, J. Su, Y. Chen, et al., Journal of Alloys and Compounds. vol.548, p.7-12 (2013); https://doi.org/10.1016/j.jallcom.2012.09.011
[24] D.-H. Lee, S. Kim, S. Y. Lee, Thin Solid Films. vol.519, p.4361-4365 (2011); https://doi.org/10.1016/j.tsf.2011.02.079
[25] G. Gupta, S. Verma, R. Nagarajan, et al., Physica B: Condensed Matter. vol.604, p.412735 (2021); https://doi.org/10.1016/j.physb.2020.412735
[26] Y. Li, Y. Li, Y. Fei, et al., Journal of Molecular Structure. vol.1261, p.132959 (2022); https://doi.org/10.1016/j.molstruc.2022.132959

[27] A. Lysak, E. Przeździecka, A. Wierzbicka, et al., Thin Solid Films. vol.781, p.139982 (2023); https://doi.org/10.1016/j.tsf.2023.139982
[28] M. N. Mia, M. F. Pervez, M. K. Hossain, et al., Results in Physics. vol.7, p.2683-2691 (2017); https://doi.org/10.1016/j.rinp.2017.07.047
[29] P. Giannozzi, S. Baroni, N. Bonini, et al., Journal of physics: Condensed matter. vol.21, p.395502 (2009); https://doi.org/10.48550/arXiv.0906.2569
[30] J. P. Perdew, K. Burke, M. Ernzerhof, Physical review letters. vol.77, p.3865 (1996); https://doi.org/10.1103/PhysRevLett.77.3865
[31] P. E. Blöchl, Physical review B. vol.50, p.17953 (1994); https://doi.org/10.1103/PhysRevB.50.17953
[32] G. Kresse, D. Joubert, Physical review B. vol.59, p.1758 (1999); https://doi.org/10.1103/PhysRevB.59.1758
[33] A. D. Becke, E. R. Johnson, The Journal of chemical physics. vol.124, p.221101 (2006); https://doi.org/10.1063/1.2213970
[34] F. Tran, P. Blaha, Physical review letters. vol.102, p.226401 (2009); https://doi.org/10.1103/PhysRevLett.102.226401
[35] M. Caglar, Y. Caglar, S. Ilican, Physica B: Condensed Matter. vol.485, p.6-13 (2016); https://doi.org/10.1016/j.physb.2015.12.049
[36] C. Boukaous, A. Telia, D. Horwat, et al., The European Physical Journal - Applied Physics. vol.65, p.20302 (2014); https://doi.org/10.1051/epjap/2013130471
[37] K. L. Foo, U. Hashim, K. Muhammad, et al., Nanoscale Research Letters. vol.9, p.429 (2014); https://doi.org/10.1186/1556-276X-9-429
[38] S. Birajdar, P. Khirade, V. Bhagwat, et al., Journal of Alloys and Compounds. vol.683, p.513-526 (2016); https://doi.org/10.1016/j.jallcom.2016.05.043
[39] O. Kalu, A. N. Abutu, H. Esparza Ponce, et al., Materials Chemistry and Physics. vol.308, p.128314 (2023); https://doi.org/10.1016/j.matchemphys.2023.128314
[40] O. Kalu, M. R. Correia, A. Cantarero, et al., Journal of Physics and Chemistry of Solids. vol.146, p.109611 (2020); https://doi.org/10.1016/j.jpcs.2020.109611
[41] O. Kalu, J. A. Duarte Moller and A. Reyes Rojas, Physics Letters A. vol.383, p.1037-1046 (2019); https://doi.org/10.1016/j.physleta.2018.11.052
[42] M. N. H. Mia, M. F. Pervez, M. K. Hossain, et al., Results in Physics. vol.7, p.2683-2691 (2017); https://doi.org/10.1016/j.rinp.2017.07.047
[43] R. Hong, J. Shao, H. He, et al., Applied Surface Science. vol.252, p.2888-2893 (2006); https://doi.org/10.1016/j.apsusc.2005.04.041
[44] O. Kalu, C. Rodríguez-Fernández, J. Cardoso, et al., Optical Materials. vol.118, p.111227 (2021); https://doi.org/10.1016/j.optmat.2021.111227
[45] J. Sengupta, A. Ahmed, R. Labar, Materials Letters. vol.109, p.265-268 (2013); https://doi.org/10.1016/j.matlet.2013.07.104
[46] K. Huang, Z. Tang, L. Zhang, et al., Applied Surface Science. vol.258, p.3710-3713 (2012); https://doi.org/10.1016/j.apsusc.2011.12.011
[47] T. Touam, M. Atoui, I. Hadjoub, et al., The European Physical Journal Applied Physics. vol.67, p.30302 (2014); https://doi.org/10.1051/epjap/2014140228
[48] C. Abed, C. Bouzidi, H. Elhouichet, et al., Applied Surface Science. vol.349, p.855-863 (2015); https://doi.org/10.1016/j.apsusc.2015.05.078
[49] P. S. Shewale, N. K. Lee, S. H. Lee, et al., Journal of Alloys and Compounds. vol.640, p.525-533 (2015); https://doi.org/10.1016/j.jallcom.2015.03.232